
# Distributed Strain Measurements in a Steel-Concrete Composite Floor Beam under Multi-Point Loading at Ambient Temperature

M. Klegseth[1], Y. Bao[2], L. Fan[1], G. Chen[1]

[1] *Department of Civil, Architectural and Environmental Engineering, Missouri University of Science and Technology, USA, Email: mak7v3@mst.edu*

[2] *Department of Civil, Environmental and Ocean Engineering, Stevens Institute of Technology, USA*

## Abstract

A 12.8 m-long composite floor beam consisting of a steel reinforced concrete slab with profiled metal decking supported by a W18×35 steel beam was tested under multi-point bending load at ambient temperature. Material strain and temperature were measured using fiber optic sensors. Measurements were taken along more than 150 m of fiber optic cables using Pre-Pump Pulse Brillouin Optical Time Domain Analysis (PPP-BOTDA) and Optical Frequency Domain Reflectometry (OFDR). Along the beam centerline, three strain and two temperature fiber loops were placed to characterize the strain and temperature distribution along and through the depth of the concrete slab. The neutral axis depth was evaluated using the measured data and compared with theoretic predictions for a fully-composite beam and a non-composite beam. The theoretic prediction was based on an elastic steel and elastic cracked concrete section and was found in general agreement with the test data.

## 1. Introduction

Neutral axis calculations are important for reinforced concrete beam design to determine the usable area of compressive strength of the section. This can be more challenging in composite steel-concrete beams than in traditional reinforced concrete because full composite action is not guaranteed between all the elements; e.g. slip can occur at the steel-concrete interface. Steel headed studs are commonly used to transfer shear forces between the steel beam and concrete slab. Full composite action is achieved if the headed studs can carry the shear load when either the steel beam has yielded or the concrete slab is stressed to its maximum compression capacity, whichever is less. When full interaction is not achieved, the beam is said to be partially composite (Vinnakota et al., 1988; Kovach 2008).

Several researchers have determined slip in composite beams as a function of the beam length for a variety of scenarios. Liu et al. (2005) determined slip and associated strain differences for a simply-supported composite beam under a concentrated load. Nie and Cai (2003) expanded this concept toward identifying the effects on the beam deflection, section modulus and investigated continuous beam behavior due to slip. Naraine (1984) investigated and related the effects of slip on the uplift of the concrete section.

## 2. Sensing Principles

Measurements were taken in the fiber optic sensors using Pre-Pump Pulse Brillouin Optical Time Domain Analysis (PPP-BOTDA). The PPP-BOTDA measurements were made using a Neubrescope 7020[1]. This method makes use of a single mode optical fiber (SMF), a modified pre-pump pulse laser, and a probe laser. The Stokes scattering process is described as the annihilation of an incident photon and the generation of a scattered photon and an induced phonon. When an intense optical field is introduced into a SMF it causes an electrostrictive force to be exerted on the particles in the medium causing an elastic acoustic wave in the fiber. This acoustic wave leads to density variations within the fiber which reacts with the incident light to cause a backscattering of light. This process is referred to as stimulated Brillouin scattering. An increased spatial resolution can be achieved if the incident light pulse from the pump laser is minimized, however the duration of the pulse must be at least 28 ns to stimulate a phonon in the medium. In PPP-BOTDA, the pump laser increases the spatial resolution by using a pre-pulse to stimulate an acoustic wave prior to the arrival of a larger pulse which is used for measurements. The backscattering light from the pump laser combines with the light from the probe laser and is recorded by a receiver that measures the intensity of the light. When the backscattering frequency is equal to the Stokes central frequency, the maximum gain is achieved. The central frequency is related linearly to strain and temperature based upon Equation (1) where the constants $C_\varepsilon$ and $C_T$ must be calibrated based upon the fiber in use (He and Liu, 1999; Kishida et al., 2004; 2014).

$$v_b = C_\varepsilon \varepsilon + C_T T \tag{1}$$

Measurements were also taken in the fiber optic sensors using Optical Frequency Domain Reflectometry (OFDR). The OFDR measurements were made using a Luna OBR 4600 - a type of Optical Backscatter Reflectometry (OBR). This technique uses swept wavelength homodyne interferometry to measure the Rayleigh backscatter throughout the length of a SMF. The Rayleigh backscatter is a property of optical fibers and is caused by radius and density fluctuations and thus index profiles throughout the length of the fiber (Soller et al., 2005; Kreger et al., 2007). Strain and temperature measurements can be obtained based upon spectral shifts in the Rayleigh spectrum which must be referenced to a baseline. The spectral shift is related linearly to temperature and strain by calibration coefficients $K_\varepsilon$ and $K_T$ (Froggatt and Moore, 1998; Rao 1997).

$$v_R = K_\varepsilon \varepsilon + K_T T \tag{2}$$

## 3. Experimental Program

The steel-concrete composite floor beam was designed and fabricated by the National Institute of Standards and Technology (NIST) as described in Ramesh et al. (2018). Relevant geometric and material properties are summarized here. As shown in Figure 1, 1.828 m-wide profiled metal decking was placed on top of a W18×35 steel beam. A lightweight aggregate concrete with polypropylene fibers was placed on top of the metal decking. A 6x6 W1.4xW1.4 welded wire

[1] Certain commercial products are identified in this paper to specify the materials used and the procedures employed. In no case does such identification imply endorsement or recommendation by the National Institute of Standards and Technology, nor does it indicate that the products are necessarily the best available for the purpose.

mesh was placed in the mid height of the concrete above the steel deck as the minimum required shrinkage and temperature control reinforcement. Composite action between the steel beam and concrete slab was achieved using 19 mm diameter headed shear studs spaced at 305 mm on center along the length of the beam. The studs were placed in a 'strong stud position' in the profiled decking and welded directly to the steel beam.

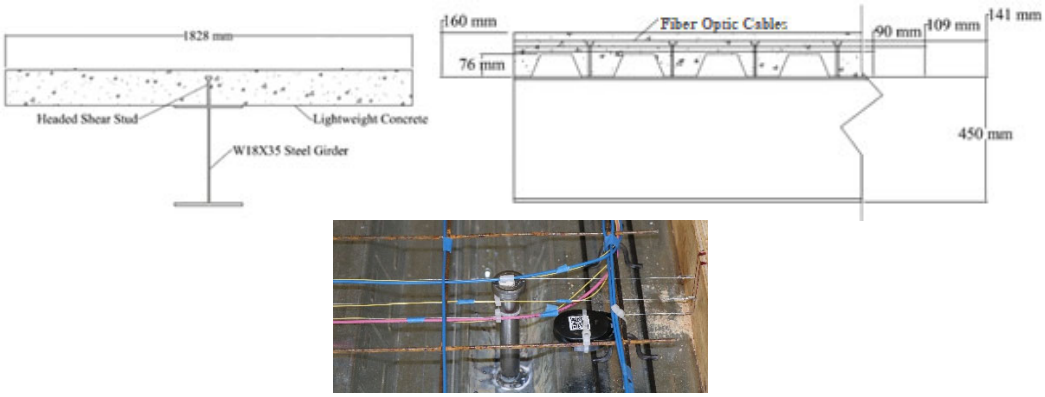


**Figure 1: Transverse and longitudinal cross sections and instrumentation scheme of the composite beam.**

Strain and temperature measurements were made using single mode optical fiber cables placed in the formwork prior to concrete casting as shown in Figure 1. The optical fibers used to measure strain (hereafter 'strain sensors') had a core diameter of 8.2 µm, a cladding diameter of 125 µm, an inner polymer coating diameter of 190 µm and an outer polymer coating diameter of 242 µm. The optical fibers used to measure temperature (hereafter 'temperature sensors') had a similar structure and cross-section dimensions, however they had an additional outer polymer jacket that allowed free movement of the measurement fiber. Three strain sensors were placed longitudinally along the centerline of the beam at heights of approximately 90 mm, 109 mm, and 141 mm up from the bottom of the slab, respectively. A temperature sensor was co-located along the bottom and top strain sensor to deconvolve the influence of temperature and strain on the measured frequency shifts (Equations 1 and 2). Additionally, two temperature sensors were run along the welded wire mesh transverse to the beam to measure temperature as reported elsewhere by Bao et al., 2017.

At each of two ends, the W18×35 beam was pin-supported through bolt connections on the load frame and subjected to six point loads along the centerline of the beam as depicted in Figure 2. Load was applied through six hydraulic actuators and transferred to the specimen by three loading/cross beams spanning the specimen at quarter points, each cross beam providing two point loads on the surface of the concrete. Each of the loading beams was connected to two actuators. The specimen was loaded in the elastic region to a constant load of 11.1 kN/actuator, 22.3 kN/actuator, and 44.5 kN/actuator.

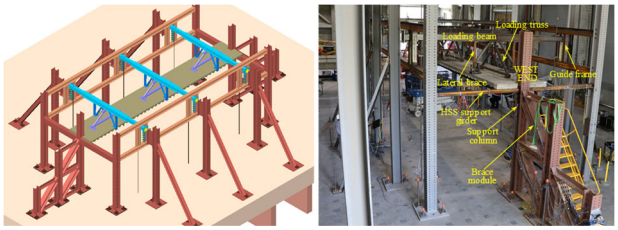


**Figure 2: A 3D schematic of the structural test setup (Ramesh et al., 2018).**

## 4. Results and Discussion

Typical strain measurements and the location of studs along the centerline of the beam for a constant applied load of 44.5 kN/actuator is shown in Figure 3. Linear regression based upon the least sum squares method was performed for the three longitudinal strain fibers as a function of distance along the beam. To account for slight misalignment of the position of fibers during data processing, a moving average was applied, which increased the effective sensor gauge length to 10 cm. Outlier data that were negative or excessively large were removed. Additionally, data that had an improper correlation between the three fibers was removed. At each cross section, the cleansed strain data was used to determine the neutral axis by linear extrapolation. The resulting neutral axis depths from these analyses are summarized in Figure 4.

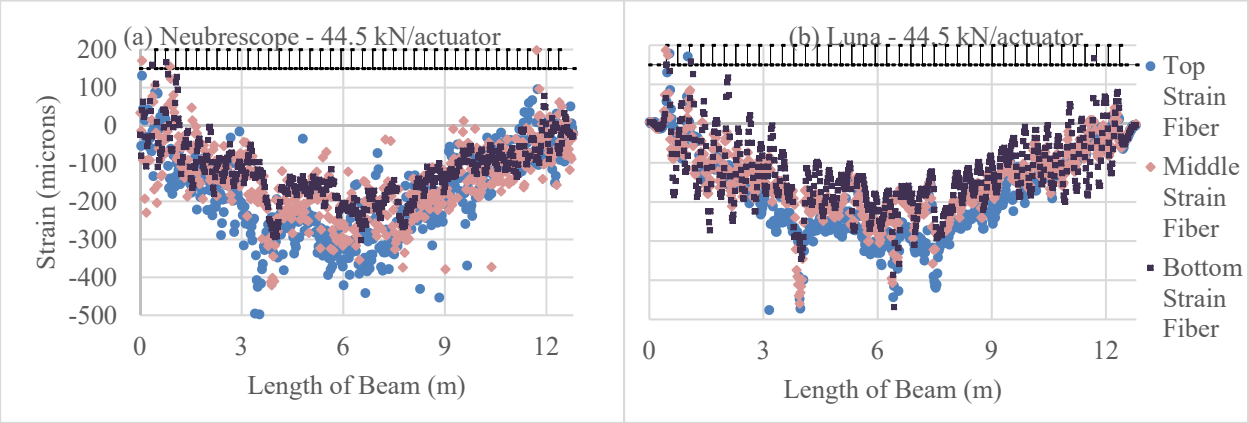


**Figure 3: Strain distribution at 44.5 kN/actuator applied load with shear studs overlayed.**

The manufacturer-provided steel tensile yield strengths for the steel beam, metal decking, shear studs, and welded wire mesh were 345 MPa, 276 MPa, 414 MPa, and 276 MPa, respectively. The elastic modulus of all steels was approximately 200 GPa. The measured density of the concrete was (1865±8.1) kg/m$^3$ and the average compressive strength of two concrete batches at 28 days was (45.4±3.5) MPa from which the modulus of elasticity of the concrete is estimated to be 23.3 GPa. Under the applied loads, both the steel and cracked concrete sections of the composite beam are assumed to remain elastic in the determination of neutral axis. Theoretical calculations show that the neutral axis is 135 mm from the top extreme fiber of concrete under full steel-concrete composite action, and 42 mm under no composite action. The maximum stress in the composite cross section was checked to ensure both the steel and concrete sections are in the elastic range under the applied loads during the laboratory tests.

Figure 4 shows a parabolic shape for the neutral axis as a function of length, suggesting that there is less composite action (more slip) near the end supports. The trend indicated in Figure 4 agrees with the theoretical and experimental work done by Naraine (1984) and Nie and Cai (2003). The local peaks in Figure 4 appear to be periodic along the length of the beam. Their potential correlation with the location of studs as indicated in Figure 4 will be investigated in future work.

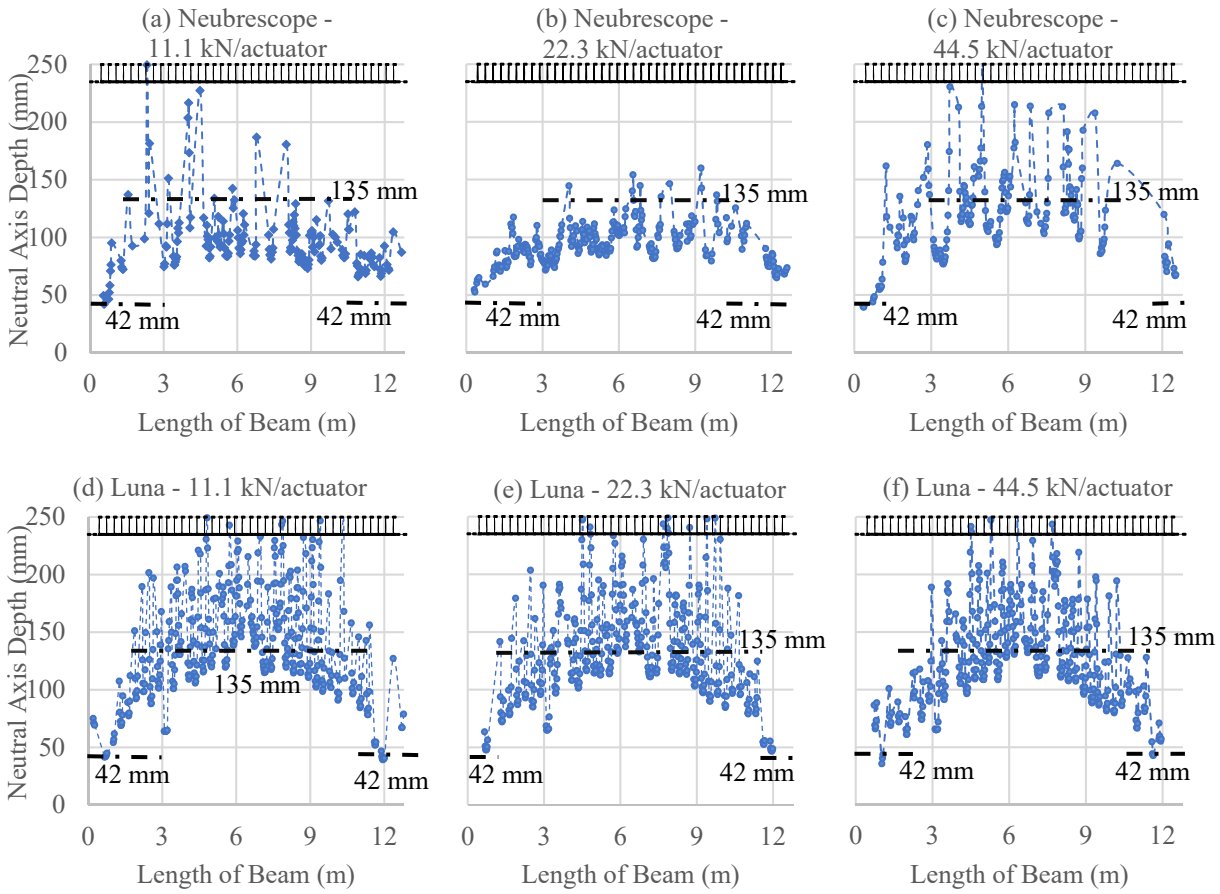


**Figure 4: Neutral axis calculation throughout the longitudinal beam length with stud location overlayed.**

## 5. Conclusion

Variation of the neutral axis depth in a composite steel-concrete slab, determined using data from distributed fiber optic strain sensors integrated in a steel-concrete composite beam, is shown. The PPP-BOTDA and OFDR sensing techniques both provided data to predict the neutral axis while simultaneously providing useful strain data. Additional tests were performed to evaluate this method for composite beam structures under simultaneous mechanical and fire load conditions for which the analysis is ongoing.

## 6. Acknowledgement

Financial support for this study is provided by the National Institute of Standards and Technology under Award No. 70NANB13H183 and the U.S. Department of Transportation, Office of the Assistant Secretary for Research and Technology (USDOT/OST-R) under Grant No. 69A3551747126 through INSPIRE University Transportation Center (http://inspire-utc.mst.edu) at Missouri University of Science and Technology. The views, opinions, findings and conclusions reflected in this publication are solely those of the authors and do not represent the official policy or position of the sponsors.

## 7. References

Bao, Y., Hoehler, M., Choe, L., Klegseth, M. A. and Chen, G. (2017). "Monitoring early-age strain and temperature distributions in full-scale steel-concrete composite beams with distributed fiber optic sensors." *Int. Workshop on Struct. Health Monit.*, Stanford, CA, 10.12783/shm2017/14023.

Froggatt, M. and Moore, J. (1998). "High-spatial-resolution distributed strain measurement in optical fiber with Rayleigh scatter." *App. Opt.*, 37(10), pp. 1735-1740, 10.1364/AO.37.001735.

He, G. S. and Liu, S. H. (1999). "Stimulated scattering of intense light." Chapter 8 in *Phys. of Nonlinear Opt.*, World Scientific Publishing Co., Singapore, pp. 175-269.

Kishida, K., Li, C.H., Lin, S. and Nishiguchi, K. (2004). "Pulsed pre pump method to achieve cm-order spatial resolution in Brillouin distributed measuring technique." Technical Report No. OFT2004-47, the Institute of Electronics Information and Communication Engineers (IEICE), 104(31), pp. 15–20, 0913-5685.

Kishida, K., Yamauchi, Y. and Guzik, A. (2014). "Study of optical fibers strain-temperature sensitivities using hybrid Brillouin-Rayleigh system." *Photonic Sen.*, 4(1), pp. 1-11, 10.1007/s13320-013-0136-1.

Kovach, J. D. (2008). "Horizontal shear capacity of composite concrete beams without interface ties." Technical Report No. 08-05, Adv. Tech. for Large Struc. Sys., Bethlehem, PA.

Kreger, S. T., Soller, B. J. Gifford, D. K., Duncan, R. G., Wolfe, M. S. and Froggatt, M. E. (2007). "Optical backscatter reflectometry as a measurement tool for fiber-optics in avionics and aerospace applications." Technical Report No. 2007-01-3863. Soc. of Auto. Eng. International, Warrendale, PA, 10.4271/2007-01-3863.

Liu, H.B., Liu, W.H. and Zhang, Y.L. (2005). "Calculation analysis of shearing slip for steel-concrete composite beam under concentrated load." *App. Math. & Mech.,* 26(6), pp. 735-740, 0253-4827(2005)06-0735-06.

Naraine, K. S. (1984). "Slip and uplift effects in composite beams." M.S. Thesis Submitted to the Graduate Faculty, McMaster University.

Nie, J. and Cai, C. S. (2003). "Steel-concrete composite beams considering shear slip effects." *J. of Struct. Eng*, 129(4), pp. 495-506., 10.1061/(ASCE)0733-9445(2003)129:4(495).

Ramesh, S., Choe, L., Hoehler, M., Grosshandler, W., and Gross, J. (2018). "Design and construction of long-span composite beam specimens for large structural-fire tests." *Proc. of Struct. Congr.*, ASCE, Forth Worth, Texas, April 19-21, 2018.

Rao, Y. J. (1997). "In-fibre Bragg grating sensors." *App. Opt.*, 8(4), pp. 355-375, 10.1088/0957-0233/8/4/002

Soller, B. J., Gifford, D. K., Wolfe, M. S. and Froggatt, M. E. (2005). "High resolution optical frequency domain reflectometry for characterization of components and assemblies." *Opt. Exp.*, 674(2), pp. 666-674, 10.1364/OPEX.13.000666.

Soller, B. J., Wolfe, M. and Froggatt, M. E. (2005). "Polarization resolved measurement of Rayleigh backscatter in fiber-optic components." *Nat. Fiber Opt. Eng. Conf.,* Anaheim, CA, 1-55752-784-9.

Vinnakota, S., Foley, C. and Vinnakota, M. R. (1988). "Design of partially or fully composite beams with ribbed metal deck using LRFD Specifications." *Eng. J.,* AISC, Second Quarter, pp. 60-78.